Lamina Cribrosa Capillaries Straighten as Intraocular Pressure Increases

Bryn L. Brazile,[1] Bin Yang,[1,2] Susannah Waxman,[1] Po Lam,[1] Andrew P. Voorhees,[1] Yi Hua,[1] Ralitsa T. Loewen,[1] Nils A. Loewen,[4] Joseph F. Rizzo III,[5] Tatjana Jakobs,[6] and Ian A. Sigal[1,3]

[1]Department of Ophthalmology, University of Pittsburgh, Pittsburgh Pennsylvania, United States
[2]Department of Engineering, Duquesne University, Pittsburgh Pennsylvania, United States
[3]Department of Bioengineering, University of Pittsburgh, Pittsburgh Pennsylvania, United States
[4]Department of Ophthalmology, University of Würzburg, Würzburg, Germany
[5]Neuro-Ophthalmology Service, Department of Ophthalmology, Massachusetts Eye and Ear and Harvard Medical School, Boston, Massachusetts, United States
[6]Department of Ophthalmology, Harvard Medical School, Boston Massachusetts, United States

Correspondence: Ian A. Sigal, Laboratory of Ocular Biomechanics, Department of Ophthalmology, University of Pittsburgh School of Medicine, 203 Lothrop Street, Eye and Ear Institute, Room 930, Pittsburgh, PA 15213, USA; ian@OcularBiomechanics.com, www.OcularBiomechanics.com.

Received: June 25, 2020
Accepted: September 8, 2020
Published: October 1, 2020

Citation: Brazile BL, Yang B, Waxman S, et al. Lamina cribrosa capillaries straighten as intraocular pressure increases. *Invest Ophthalmol Vis Sci.* 2020;61(12):2. https://doi.org/10.1167/iovs.61.12.2

Purpose. The purpose of this study was to visualize the lamina cribrosa (LC) capillaries and collagenous beams, measure capillary tortuosity (path length over straight end-to-end length), and determine if capillary tortuosity changes when intraocular pressure (IOP) increases.

Methods. Within 8 hours of sacrifice, 3 pig heads were cannulated via the external ophthalmic artery, perfused with PBS to remove blood, and then perfused with a fluorescent dye to label the capillaries. The posterior pole of each eye was mounted in a custom-made inflation chamber for control of IOP with simultaneous imaging. Capillaries and collagen beams were visualized with structured light illumination enhanced imaging at IOPs from 5 to 50 mm Hg at each 5 mm Hg increment. Capillary tortuosity was measured from the images and paired two-sample *t*-tests were used to assess for significant changes in relation to changes in IOP.

Results. Capillaries were highly tortuous at 15 mm Hg (up to 1.45). In all but one eye, tortuosity decreased significantly as IOP increased from 15 to 25 mm Hg ($P < 0.01$), and tortuosity decreased significantly in every eye as IOP increased from 15 to 40 mm Hg ($P < 0.01$). In only 16% of capillaries, tortuosity increased with elevated IOP. Capillaries had a surprisingly different topology from the collagen beams.

Conclusions. Although high capillary tortuosity is sometimes regarded as potentially problematic because it can reduce blood flow, LC capillary tortuosity may provide slack that mitigates against reduced flow and structural damage caused by excessive stretch under elevated IOP. We speculate that low capillary tortuosity could be a risk factor for damage under high IOP.

Keywords: optic nerve head, collagen, vasculature, lamina cribrosa, intraocular pressure, tortuosity, capillaries

Glaucoma causes permanent and sometimes disabling blindness to millions of people worldwide,[1–3] yet the causes of glaucomatous neuropathy are not fully understood. Susceptibility to glaucoma is thought by some to be related to vascular dysfunction within the optic nerve head (ONH), specifically within the lamina cribrosa (LC) region.[4–7] In addition, elevated intraocular pressure (IOP) can lead to a mechanical insult of the LC region,[8–13] which could disrupt the LC vasculature and could cause ischemia.[14–17] Elevated IOP is the only modifiable risk factor for glaucoma and the reduction of IOP is the only accepted treatment for slowing the progression of visual field loss,[18–20] potentially by reducing the mechanical burden on the LC.[8–15] Overall, a larger IOP-induced mechanical insult is thought to translate into a higher likelihood of neural tissue damage.[21,22] As mechanical insult within the LC increases, retinal ganglion cell (RGC) axons are compressed or sheared, potentially affecting their axoplasmic transport.[11,14] In addition, increased mechanical insult leads to stretch-induced activation of astrocytes.[16,23–27] However, the direct effects of this mechanical insult on the vasculature within the LC region remain unclear.

The LC is a highly vascular structure in which the blood vessels, 10 to 20 um in diameter, have been described to lie in the collagen beams and form a dense capillary plexus.[28,29] However, there is very limited information available on how the vasculature is intertwined with the collagen beams or how the vasculature interacts with the RGC axons within the LC. Furthermore, very little information is known about the general characteristics of these capillaries.

Although there are several potentially important capillary characteristics, tortuosity, defined as path length over straight end-to-end length, has been shown useful in

the study of microvascular geometry and perfusion in other tissues. Studies have shown, for instance, that capillary tortuosity significantly affects oxygen exchange within tissues.[30–35] A single more tortuous capillary can be in close proximity to a larger volume of tissue than a straight capillary of the same end-to-end length. An increased capillary-to-tissue ratio may allow for greater maintenance of oxygen exchange. However, with each turn and loop of tortuous capillaries, there is a loss of energy such that increased blood pressure is needed to maintain flow in these vessels.[36,37] In aged and diseased brains, there is a noticeable increase in capillary tortuosity, which leads to increases in the capillary length between branch points and to decreases in the ratio between capillary density and neuronal density in addition to retarding blood flow.[37–39] Computational models of oxygen transport under physiological conditions in striated muscle, on the other hand, have shown that increased capillary tortuosity enhances oxygen transport to the surrounding tissues.[33]

In vivo measured capillary tortuosity changes have been studied in the retina as it relates to diseases, such as cardiovascular disease, systemic hypertension, and diabetes mellitus.[40–42] However, despite recent advances in in vivo imaging, particularly optical coherence tomography angiography (OCT-A),[43–45] limitations in signal penetration and resolution still prevent comprehensive visualization of the vasculature inside the LC and retrolaminar regions. Thus, how the vasculature in these regions, specifically within the LC region, deforms in response to changes in IOP remains unknown. This knowledge would seem to be essential to understand the pathophysiology of glaucoma. Hence, our goal for this study was to visualize the capillaries in the LC, measure each capillary tortuosity, and determine how changes in IOP affect the tortuosity of capillaries in the LC.

Methods

Capillary Labeling

Porcine heads (6 months old) were obtained from a local abattoir within 8 hours of death. The lower jaw and muscles were dissected away to gain access to the external ophthalmic artery. A small silicone rubber tube of 1 mm outside diameter was inserted and the proximal end of the artery was ligated closed. The vascular bed of the eye was perfused with PBS to flush out residual blood and to remove blood clots within the vascular bed. Vasculature was perfused with PBS until the perfusate was clear. This PBS wash was followed by 50 mL of an aqueous solution of DiI, which was freshly prepared from a stock solution of 6 mg/mL DiI in N,N-Dimethylformamide, and diluted to the final concentration of 120 µg/mL in PBS solution with 5% glucose to adjust for osmolarity. The DiI solution was perfused at a rate of 5 to 10 mL per minutes for 10 minutes, which was followed by a second PBS wash until the perfusate was clear.

Once the perfusion was complete, a suture was placed within the conjunctiva approximately 3 mm from the limbus to maintain eye orientation. The eyes were enucleated and cleaned of extraocular tissues. Each eye was hemisected into anterior and posterior sections to perform an initial check of the capillary labeling by observing the retinal and choroidal vessels. If the retinal and choroidal vessels were not brightly labeled, the eyes were set aside and not considered for the analysis in this report. This occurred in fewer than 15% of the eyes studied. The ONH was isolated with a 16 mm trephine. To improve visualization of the LC region, the retina and superficial prelaminar tissues were carefully removed with micro-dissecting scissors and forceps under a dissecting microscope. After these tissues were removed, another perfusion check was performed, and only eyes that had at least 30 capillaries labeled within the LC were utilized for this experiment.

Inflation Setup

The ONH was placed onto the anterior chamber of a custom-made inflation device with the ONH, specifically, the LC, centered in the viewing window. This viewing window allows for simultaneous illumination and imaging while controlling the IOP. A clamping disc was placed onto the anterior chamber around the edge of the posterior pole to create a pressure seal. Finally, the posterior base, which locks the inflation device together and contains a chamber to keep the posterior side of the eye hydrated, was attached (Fig. 1A).

The anterior chamber and posterior base were both carefully filled with PBS to ensure no air bubbles remained. The pressurization ports on the anterior chamber were connected to a PBS fluid column for IOP control and an in-line pressure transducer for IOP recording. The fluid column was set to 5 mm Hg and a wait time of 15 minutes was used to ensure tissue viscoelastic equilibration before imaging. For each eye tested, a step-wise pressure ramp was performed from 5 mm Hg to 50 mm Hg in steps of 5 mm Hg. After each pressure step, a 15-minute equilibration time was observed before acquiring the images.

Image Acquisition

The labeled vasculature and LC collagen beams were imaged using a recently developed structured polarized light microscopy (SPLM) imaging system.[46] Briefly, the images were acquired using an Olympus MVX10 upright microscope (6.3× magnification setting) with a scientific-grade camera (Hamamatsu, Flash 4.0 LT) and a 1× objective (numerical aperture [NA], 0.25) at an effective magnification of 6.3×. Structured light illumination was achieved with a digital light projector (LightCrafter evaluation module; Texas Instruments). The projection axis was aligned at 30 degrees to the imaging axis (Fig. 1B). Imaging was performed as described elsewhere.[46] Briefly, for each IOP step, three 2D-sinusoidal patterns with a phase shift of 0 degrees, 120 degrees, and 240 degrees were projected onto the sample sequentially and corresponding reflectance or fluorescence images were acquired. The spatial frequency was 3 mm^{-1}.[46] Both pattern projection and image acquisition were controlled by a custom LabVIEW program. For image acquisition, first, the collagen beams were brought into focus and imaged, then, we switched to the fluorescence filter and acquired the capillary image. This was repeated for each IOP step in the pressure ramp. At each IOP step, we derived images using the SPLM demodulation process described previously.[47] Specifically, we used the so-called AC image, which enhances collagen visibility in reflectance and enhances the depth resolution of the fluorescence. The DC component of the SPLM process was not used. The beam

Investigative Ophthalmology & Visual Science

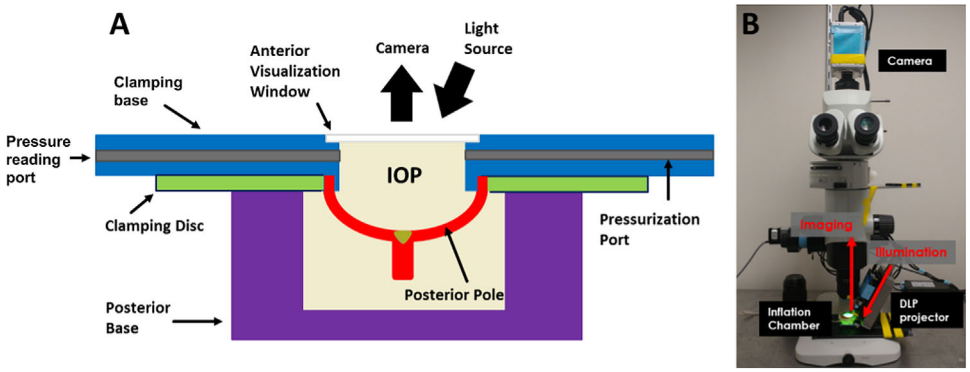

Figure 1. (**A**) Illustration of a posterior pole mounted inside the custom-made inflation chamber. The posterior pole was clamped between the clamping base (*blue*) and the clamping disc (*green*). Imaging was done from the front while intraocular pressure was measured and controlled. The globe interior was filled with saline, whereas the exterior was kept hydrated and at room pressure. This is a diagram and is not to scale. (**B**) Photograph of the imaging setup.

and capillary AC images can be merged into one image to visualize the changes that occur as IOP is increased.

Image Analysis

Analyses for 15, 25, and 40 mm Hg were performed as these are representative of physiologic, elevated, and very high IOP seen in the clinic. To analyze the change in the vasculature at each IOP setting, the capillaries in each eye were manually traced in the software package Fiji[48] for each acquired capillary AC image. Individual capillaries were defined as unbranched vascular tracts between two branch points or between a branch point and a terminal point. This length of the capillary trace was divided by the end-to-end distance of the capillary to obtain each capillary's tortuosity. Each eye's capillary tortuosity was compared for each IOP step. Due to limited axial resolution and high lateral resolution, all measurements of tortuosity were conducted on 2D images. The 3D information was taken into account only to distinguish capillaries in different planes from one another.

Statistical Analysis

1) *Repeatability of manual marked tortuosity measurements.* To determine the repeatability of measuring the capillary tortuosity in the capillary AC images of an eye, the marker was asked to measure the same 20 capillaries in an eye 3 times. These 20 capillaries were chosen at random from all easily visible capillaries. The standard deviation of the marker's three tortuosity measurements was calculated. One marker scored samples throughout the study (B.B.). The marker was not masked to eye status.
2) *Individual eye differences in capillary tortuosity.* Two-sample paired *t*-tests were used to determine if the change in capillary tortuosity was significant for each IOP step in each individual eye. Results were considered significant when $\alpha = 0.01$.
3) *Population differences in capillary tortuosity.* Linear mixed effect models accounting for autocorrelation of measurements from the same eye were used to determine if there were significant associations between IOP and capillary tortuosity pooled across all eyes. A significance level of $\alpha = 0.01$ was used.

Results

Upon enucleation, the extraocular fat and muscles surrounding the eye were noticeably stained pink by the DiI (Figs. 2A, 2B). After hemisection, the LC collagen beams were visible behind the neural tissue, and the retinal and choroidal vessels appeared brightly labeled (Figs. 2C, 2D). Capillaries were readily traced and tortuosity was calculated by dividing the length of the capillary trace by its end-to-end distance (Fig. 2E). Merged collagen beam and capillary AC images at 15 mm Hg (Fig. 3) are shown to highlight the differences in how both structures spanned the optic nerve. LC capillaries could be tracked throughout the LC at multiple IOPs. Intraocular pressure-induced capillary deformations are highlighted through overlay of capillaries at 15 and 40 mm Hg (Fig. 4). A gif was then created with these merged images at each IOP step to highlight how each structure responded as IOP was increased.

The marker was directed to identify the same 30 capillaries in an eye 3 times. The standard deviation of the marker's three sets of capillary tortuosity measurements was 0.014. Depth-encoded projection images best allowed for interpretation of capillary branch points and paths, which could not otherwise be determined in depth-agnostic projections (Fig. 5). At 15 mm Hg, the LC capillaries were highly tortuous (up to 1.45). As IOP increased, the overall tortuosity of the capillaries decreased for all eyes (Fig. 6). For every eye, there was a statistically significant ($P < 0.01$) lower tortuosity at 40 mm Hg than at 15 mm Hg. For all but one eye, there was a statistically significant ($P < 0.01$) lower tortuosity at 40 mm Hg than at 25 mm Hg. Eye #6 also showed a statistically significant drop in capillary tortuosity from 15 mm Hg to 25 mm Hg. When looking at the pooled capillary measurements of all eyes, the linear mixed effect model also showed that the decrease in tortuosity as IOP increased was statistically significant ($P < 0.01$).

Further examination of each eye's capillary tortuosity revealed that not every capillary experienced a decrease in tortuosity. Some capillaries had very little change; whereas, a few capillaries became more tortuous as IOP increased, as shown in the scatter plot in Figure 7. The orange dots represent individual capillaries in eye #3; whereas the blue dots represent individual capillaries in eye #6.

Investigative Ophthalmology & Visual Science

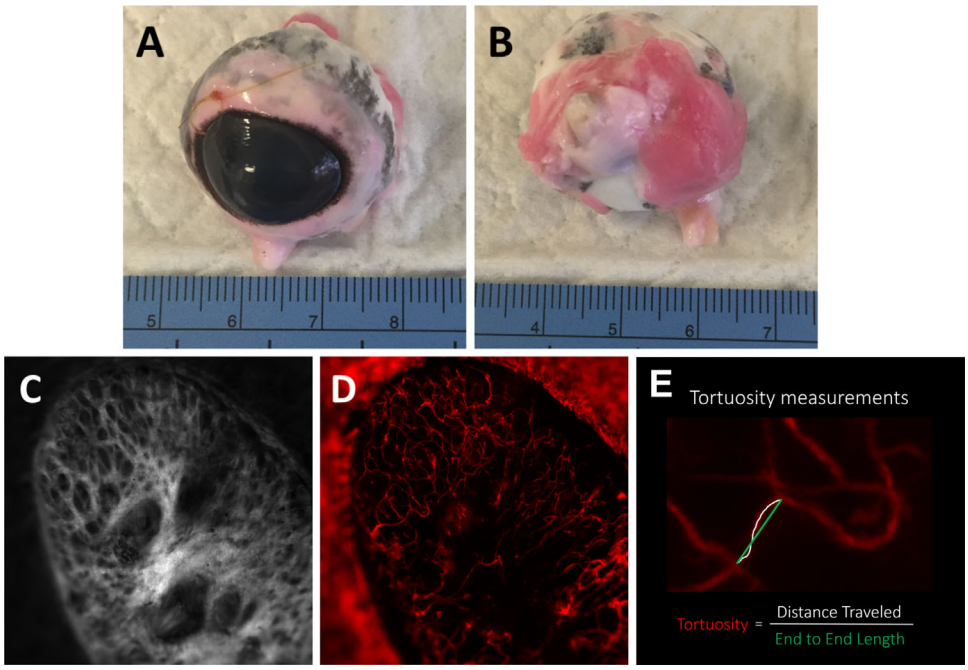

Figure 2. Enucleated porcine eye with vessels labeled with DiI. Images of (**A**) anterior portion of the eye and (**B**) posterior portion of the eye show the vessels of the extraocular fat and muscles dyed pink with DiI. (**C**) Structured light AC image of the collagen beams of various sizes spanning the LC acquired at 6.3× after the prelaminar tissues have been removed. (**D**) Structured light fluorescence AC image of the DiI labeled vessels in the LC *pseudo-colored red*. (**E**) Individual capillaries traces were created between branch-points. Tortuosity was calculated by dividing the distance traveled by a capillary trace (*white line*) by the end to end length of the trace (*green line*).

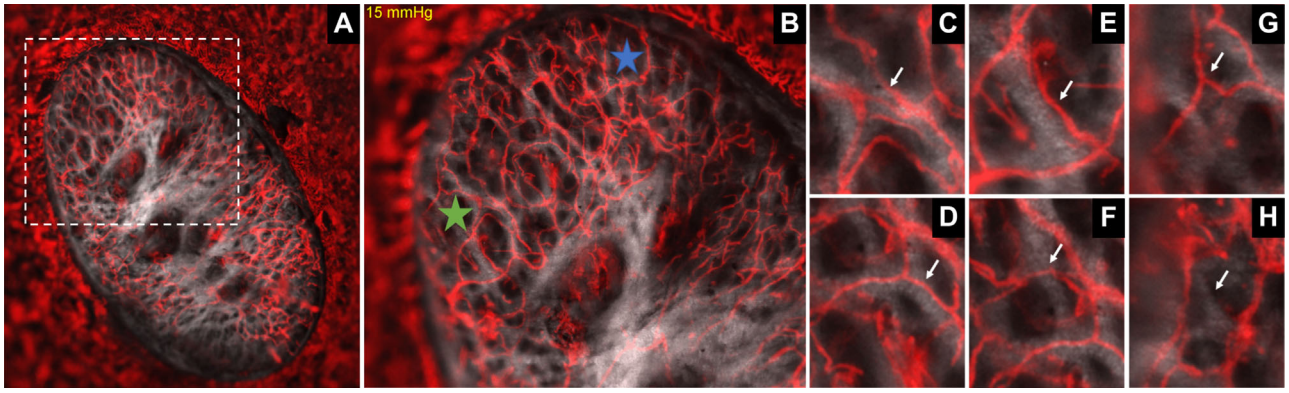

Figure 3. (**A**) Merged 6.3× image of the collagen beams (*gray*) and labeled capillaries (*red*) of a porcine eye at 15 mm Hg. (**B**) Detail of the region within the *dashed lines* in **A**. There are distinct differences between the beams and the capillaries. There are areas in the LC with high (capillaries near *blue star*) and low (capillaries near *green star*) capillary density. Other interesting observations are highlighted with *white arrows* in close-ups panels (**C–H**). **C** Beams that have multiple capillaries inside them. **D** Beams with single capillaries inside. **E** Capillaries that run along the outside of a beam. **F** Capillaries that cross perpendicularly to a beam. **G** Capillaries inside of the pores without any beam support. **H** Beams without any capillaries.

Discussion

Extensive biomechanical modeling efforts have been directed toward understanding how IOP-induced deformation of the LC impacts retinal ganglion cell axon damage. What has not been factored into these studies is how deformations affect the form and path of capillaries that supply the tissue. With decreased blood flow and impaired hemodynamic regulation observed early in the pathogenesis of glaucoma, vascular dysfunction has been proposed to be a mechanism of pathology.[49–51] The bulk of vascular resistance resides in capillaries and the extent of capillary tortuosity can affect perfusion. However, the structure of LC capillaries has not been investigated in relation to that of collagen beams at physiologic and pathologically elevated IOPs. For this reason, we aimed to investigate the effect of IOP on LC capillary tortuosity.

To accomplish this, we visualized capillaries and extracellular matrix (ECM) in the porcine LC, measured each capillary's tortuosity, and determined if tortuosity changes are associated with IOP changes. This was achieved by utilizing a recently developed imaging technique based on structured light illumination to simultaneously image the LC collagen beams and capillaries while also controlling

Investigative Ophthalmology & Visual Science

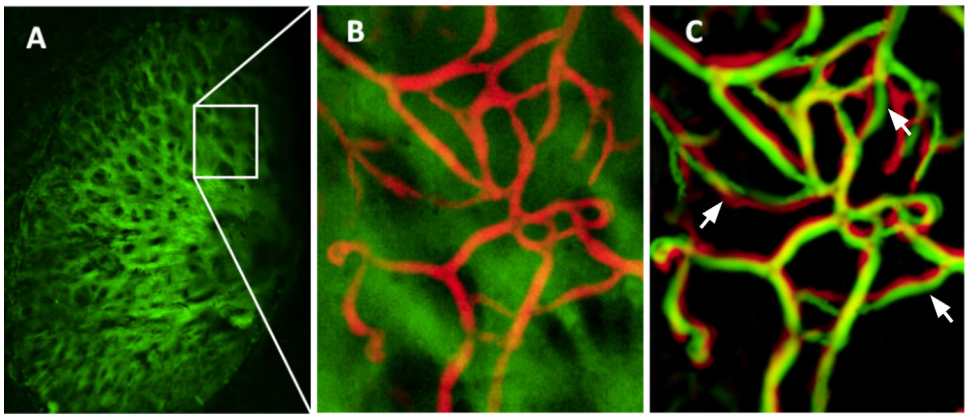

Figure 4. (**A**) lamina cribrosa extracellular matrix (*green*) as visualized via structured light illumination. (**B**) Overlay of capillaries (*red*) and collagen beams (*green*) at 15 mm Hg. (**C**) To illustrate deformations with IOP, capillaries are shown in *red* at 15 mm Hg, in *green* at 45 mm Hg, and in *yellow* where they overlap. *White arrows* indicate representative vessels in which the IOP increase caused pronounced changes in tortuosity.

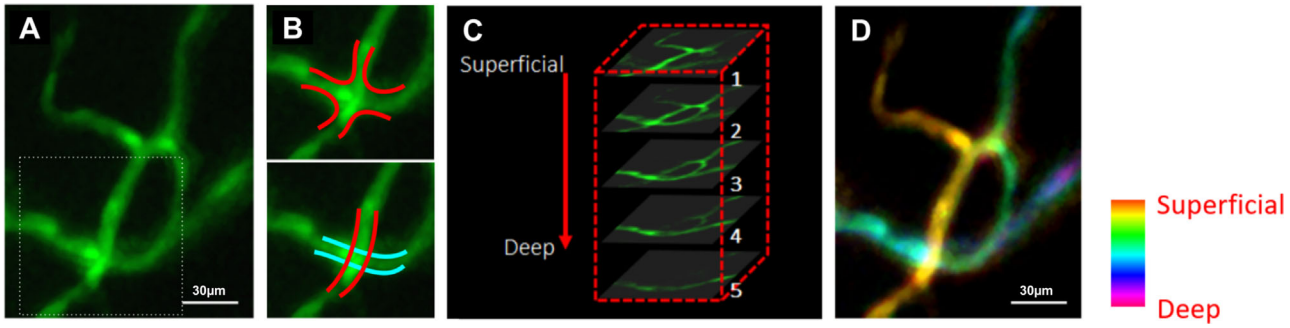

Figure 5. Use of 3D information to improve capillary identification. (**A**) An example of the 2D visualization of LC capillaries (*green*) exhibits an ambiguity. It is not clear whether the tracts in the *dashed box* intersect to create a loop (**B**, *top*) or if one tract exists at a different plane of depth than the other **B**, *bottom*. (**C**) Depth-resolved images of this region allow for interpretation of the capillary's path. (**D**) A depth-encoded projection reveals that capillaries do not intersect as the depth-agnostic projection may misleadingly suggest. One portion of the capillary is more superficial (*orange*) than the other (*green-blue*) and the two do not physically meet. Scalebars denote 30 μm. As per our definition of capillary segments between branches, in this work, these would be considered two separate capillaries.

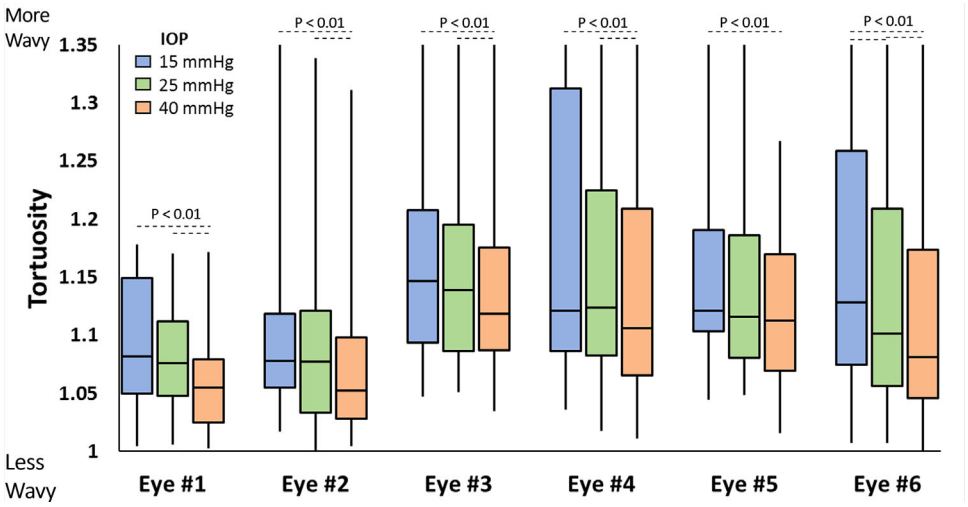

Figure 6. Boxplots of the capillary tortuosity for each eye at each IOP step. Individual eye tortuosity was highly variable. Overall tortuosity decreased as IOP increased. Statistically significant decreases ($P < 0.01$) were determined via two sample paired *t*-tests and are indicated with *dashed lines*. All eyes experienced a statistically significant drop in capillary tortuosity as IOP increased from 15 mm Hg to 40 mm Hg. All but one eye experienced a statistically significant drop in capillary tortuosity as IOP increased from 25 mm Hg to 40 mm Hg.

Investigative Ophthalmology & Visual Science

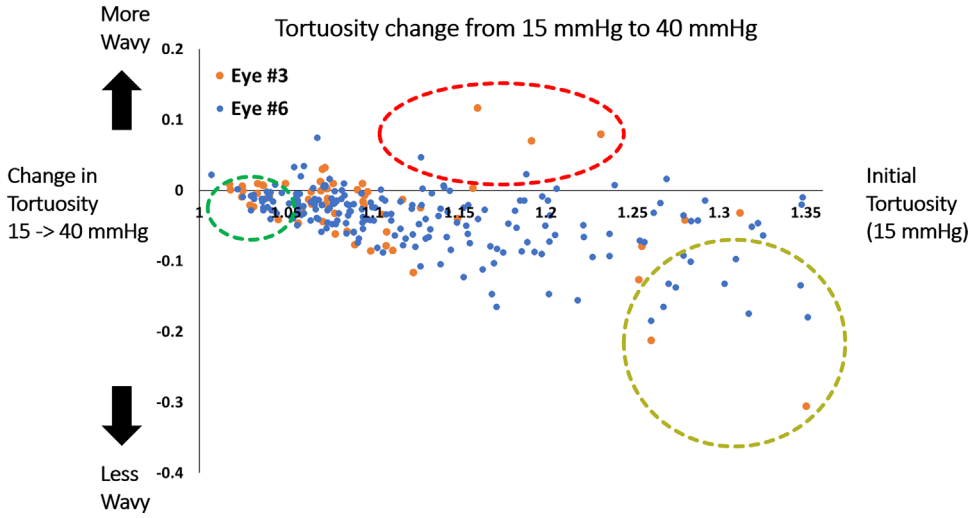

Figure 7. Scatter plot highlighting representative differences in tortuosity measurements of individual capillaries taken at 15 mm Hg and 40 mm Hg for 2 eyes. A dot represents the total change in the tortuosity from 15 mm Hg to 40 mm Hg for one capillary. Dots below the *horizontal line* represent a capillary that had a decrease in tortuosity or became straighter, and *dots* above the horizontal represent capillaries that increased in tortuosity or became wavier. The *green circle* indicates capillaries that start out nearly straight and become straighter as IOP increased. The *tan circle* highlights capillaries that experienced the greatest overall decrease in tortuosity as IOP increased. The *red circle* shows capillaries that became more tortuous as IOP increased.

IOP. Focus was placed on findings at IOPs of 15, 25, and 40 mm Hg, which clinically represent IOP levels that would be considered physiologic, elevated, and very high, respectively. We present three key findings from this work. First, structured light illumination and the vascular labeling technique utilized here is well-suited for visualization of LC collagen beams and capillaries for ex vivo analysis. Second, each eye experienced a statistically significant decrease in capillary tortuosity as IOP increased from 15 to 40 mm Hg. Third, even though overall tortuosity decreased as IOP increased, some capillaries became more tortuous as IOP increased. Each of these key findings is discussed in more detail below.

Structured light illumination and DiI perfusion allowed in situ visualization of LC capillaries and collagen beams ex vivo. Perfusion of DiI resulted in relatively evenly distributed fluorescent labeling of vasculature, indicating successful delivery of label and little to no vascular obstruction. Vascular labeling successfully withstood the time and variety of intraocular pressures required over the course of this study. Depth resolution aided in distinguishing between branch points of capillaries and capillaries that only appeared to intersect when viewed in projection, a point of particular importance in evaluating tortuosity of individual capillaries. For these reasons, this pipeline lends itself well to time-series evaluation of LC capillary form. Additionally, this system allows for imaging of both collagen beams and capillaries in the same field of view. Ongoing research is being conducted to detail the intricate relationships between these two networks ex vivo.

Overall capillary tortuosity decreased as IOP increased. Capillary tortuosity at 15 mm Hg varied across the LC within each eye. As IOP was increased, the lamina canals expanded, stretching the lamina beams and capillaries. This structural change resulted in an overall lower capillary tortuosity across the LC. Decrease of vascular tortuosity may be related to IOP-induced LC deformation, particularly in the case of LC curvature.[52] Although high tortuosity in capillaries is often regarded as problematic because of increased intravascular resistance that would reduce blood flow,[53] in the LC the higher tortuosity at 15 mm Hg may provide "slack" that protects the capillaries from over-stretch damage and detrimental narrowing under elevated IOP. We thus speculate that low tortuosity capillaries could be a risk factor for damage.

Even though overall tortuosity decreased as IOP increased, some capillary segments became more tortuous. When looking more closely at individual capillaries, we noticed three interesting scenarios. First, capillaries with very high initial tortuosity became almost completely straight as IOP reached 40 mm Hg. These capillaries could be sites where blood flow is altered, which could compromise delivery of oxygen and other nutrients to the surrounding neural tissues. Second, as mentioned above, there were capillaries with low tortuosity at 15 mm Hg IOP. These capillaries then stretched as IOP increased, which, if stretched too far, could damage the capillaries and cause hemorrhages clinically.[54,55] Finally, we noticed that 16% of the capillaries became more tortuous as IOP increased. These capillaries could also be a site of altered blood flow in which blood cells pass through these capillaries much more slowly than at normal IOP. Each of these three scenarios could be potential mechanisms that lead to RGC axon loss, and future studies should examine the neural consequences of these mechanisms.

Over the last 2 decades, researchers studying ONH vasculature have largely switched to noninvasive in vivo imaging technologies, especially fluorescein angiography (FA) and OCT-A. FA provides useful images of retinal blood vessels.[56,57] However, FA is limited to only studying the superficial layers of the ONH and does not have the depth penetration to image the vasculature of the lamina and retrolaminar regions. OCT-A allows imaging of capillary perfusion within the ONH without the need for dye injection, and this technique recently revealed that a glaucomatous eye had decreased flow signals within the LC when compared to

a normal eye.[45] However, even the most advanced version of swept source OCT-A can only obtain blood flow signals when the LC is clearly visible. Projection artifacts must be removed from surface vessels, and tissue cannot image deeply enough to capture the entire laminar and retrolaminar capillary beds that are likely relevant to the pathogenesis of not only glaucoma but non-arteritic anterior ischemic optic neuropathy (NAION) as well.[58,59] Application of a compensation algorithm to OCT images of the ONH greatly enhanced contrast, reduced blood-vessel shadows, and allowed for better visualization of the deeper portions of the ONH, but is not sufficient for LC visualization of vasculature or blood flow.[60] Other techniques, including optoacoustic, ultrasound, magnetic resonance imaging (MRI), and micro-computed tomography (CT) have excellent signal penetration but lack the spatial resolution required for detailed analysis of the LC.[61–65] Thus, ex vivo studies remain a necessary way to study the effects of IOP on the LC and retrolaminar vasculature.

Although we are not the first to look at the blood vessels in the ONH or the LC, to the best of our knowledge, we are the first to measure direct deformation of LC capillaries in response to changes in IOP. In the 1980s and 1990s, several research groups studied vascular casts of the ONH.[66–68] With their method, a plastic casting agent is perfused through the vasculature and allowed to set. The tissues are then digested, leaving a cast of only the vasculature. There are several limitations to this method. First, it cannot be used to capture the relationship between the connective tissue and the vasculature. Second, due to the high viscosity of the casting agents, casting methods require intravascular injections under relatively high pressure, which may expand vestigial connections that are not functional during life, which, it has been argued, can lead to spurious interpretations.[69] Recently, confocal imaging of thick sections has been used to look at capillary and RGC axon density.[70] This method also lacks the ability to image the vasculature at multiple levels of IOP, but it has the benefit of being able to label capillaries and other tissues that the plastic cast method removes. Others have been able to investigate the effects of IOP on ONH vessel function in live rats through OCT-A.[44] Whereas in vivo measurements are particularly valuable, our studies utilize ex vivo porcine ONHs, which are more similar in size and collagen distribution to those of humans. Additionally, the method presented here allowed for tracking changes in vessel shape as IOP was increased. The resolution of OCT would not readily allow for this. Photo acoustic imaging has also been proposed to study the pig LC vasculature,[71] where the relatively high temporal resolution may allow study of perfusion and biomechanics. However, the technique provides no information on the collagen structure, has relatively low resolution, and is potentially susceptible to artifacts from pigment.

In our approach, low-viscosity aqueous solutions are perfused through the central retinal artery (CRA) and ciliary arteries at controlled lower pressures after extensive flushing blood from the tissue. This both minimizes artifactual vessel expansion and maximizes the ease of perfusion to all available tracts. However, we acknowledge that any method of intravascular perfusion could fail to identify some poorly perfused vessels. In future studies, the use of anticlotting agents may further increase confidence in achieving a more complete perfusion. Additionally, comparison of ex vivo findings with those from histological observation can serve as a supplementary method of characterization. In these studies, the density and distribution of capillaries observed through our method was consistent with what has been previously reported. Importantly, our method does not require tissue to be digested or removed to visualize the LC vasculature, which makes it possible to more clearly study the relationships between the ECM and capillaries of the LC at various IOPs.

It is important to consider the limitations of our study together with its strengths. The tissues used in this study were healthy, mature ex vivo porcine eyes. Although similar to human eyes in respect to their size and collagenous LC, porcine eyes have distinct structural differences from human eyes, such as having multiple central retinal arteries and veins. In addition, it remains to be established whether the LC vasculature is truly comparable between pigs and humans. Intravascular perfusion of dyes in human donor globes has been successfully accomplished by others[72] and would require optimization for adaptation to our technique. Future work should include additional animal models, investigation of human eyes, eyes of different ages, and diseased eyes to further understand the LC vasculature. Additionally, our ex vivo findings of the effects of IOP-induced deformations are independent of the impact of neurovascular coupling and blood pressure within capillaries, which presumably are relevant parameters for neural health. Vascular tone, particularly in large vessels, does impact tissue biomechanics and thus the absence of blood pressure likely affects the mechanics of the LC to some degree. Given the low physiological pressure in these capillaries,[73,74] the effects of capillary stiffening would be minimal and have little to no effect on its tortuosity.

It must be recognized that perfusion of vasculature ex vivo may not reach all vascular tracts. This can be due in part to clotting and/or insufficient perfusate volume. In an effort to prevent vascular obstruction and visualize as many vessels as possible, efforts were taken to minimize time between death of the animal and time of perfusion. Extensive flushing of vasculature with PBS was performed to remove blood from tissues. A large volume (50 mL) of dye was perfused for each eye in an effort to help ensure sufficient labeling. Eyes were screened under a fluorescence microscope for strong labeling of retinal and choroidal vessels prior to experiments. All eyes demonstrated continuous staining of vessels and did not show any notable leaks. Whereas the presence of unlabeled vessels is possible, we believe that we labeled the majority of vessels present. Additionally, lack of labeling in some vessels does not affect the main conclusions of this study.

Our measurements of the LC vasculature were performed in pig eyes with the prelaminar tissue removed, as prelaminar tissue can hamper visualization of LC microstructure.[75] To minimize this risk of LC damage, we used very fine microdissecting scissors and forceps to remove these tissues under a dissecting microscope. In addition, we erred on the side of caution when removing these tissues so that the LC remained intact. Last, the capillary measurements were taken from a single snapshot or projection of the vasculature, which is a complex 3D structure. Future studies should include depth resolution of the LC vasculature when quantifying these capillaries, potentially utilizing more advanced SLI techniques to obtain the 3D data on the LC vasculature. A dedicated and comprehensive comparison of the vascular and collagenous networks of the LC is beyond the scope of this work. Although these measurements were made on limited 2D images, these results are still significant as they

Investigative Ophthalmology & Visual Science

are the first to capture the changes in tortuosity of capillaries within the LC as IOP increases.

Impairment of blood flow has been found in the ONH of glaucomatous eyes and eyes with elevated IOP.[76,77] Vascular tortuosity may be a key factor associated with or affecting these changes in blood flow. In larger vessels, increases in tortuosity are known to be associated with various pathologies and can increase resistance to flow.[53] At the capillary scale, this relationship is more complex. Further work is needed to draw conclusions about the extent to which microvascular tortuosity may impact blood flow in the LC. In the event that capillary tortuosity has no or limited effects on blood flow in the LC, this remains a valuable finding, as we know to search elsewhere for signs and causes of optic nerve degeneration.

In conclusion, we have presented novel measurements of the tortuosity of capillaries inside the LC at multiple IOPs. Our measurements show that tortuosity and IOP are inversely associated. As IOP was increased, we observed a significant decrease in capillary tortuosity, thus likely altering or even compromising the blood flow in the LC. This can disrupt the vital delivery of oxygen and other nutrients to the neural tissues. Similarly, our results demonstrated that LC collagen beams and capillaries have different topological paths across the ONH, which is likely due to vastly different roles of these two structures. Because the capillary topology is so different from the collagen beams, this may allow astrocytes and other neural tissues access to these capillaries, and that areas with low capillary density may be more at risk than areas with high capillary density. This study emphasizes the need to continue the development of improved methods to image and measure LC vasculature.

Acknowledgments

Supported by National Institutes of Health R01-EY023966, T32-EY017271, and P30-EY008098; Eye and Ear Foundation (Pittsburgh, Pennsylvania), Research to prevent blindness (funds to the Department of Ophthalmology at the University of Pittsburgh).

Disclosure: **B.L. Brazile**, was at the University of Pittsburgh when he contributed to this work. He is now at Baxter (E); **B. Yang,** None; **S. Waxman**, None; **P. Lam**, None; **A.P. Voorhees,** was at the University of Pittsburgh when he contributed to this work. He is now at Johnson & Johnson Vision (E); **Y. Hua,** None; **R.T. Loewen**, None; **N.A. Loewen**, None; **J.F. Rizzo** III, None; **T. Jakobs**, None; **I.A. Sigal**, None

References

1. Cook C, Foster P. Epidemiology of glaucoma: what's new? *Can J Ophthalmol*. 2012;47:223–226.
2. Bourne RRA, Taylor HR, Flaxman SR, et al. Number of people blind or visually impaired by glaucoma worldwide and in world regions 1990–2010: a meta-analysis. *PLoS One*. 2016;11:e0162229.
3. Wang W, He M, Li Z, Huang W. Epidemiological variations and trends in health burden of glaucoma worldwide. *Acta Ophthalmol*. 2019;97:e349–e355.
4. Quigley H, Anderson DR. The dynamics and location of axonal transport blockade by acute intraocular pressure elevation in primate optic nerve. *Invest Ophthalmol*. 1976;15:606–616.
5. Quigley HA, Anderson DR. Distribution of axonal transport blockade by acute intraocular pressure elevation in the primate optic nerve head. *Invest Ophthalmol Vis Sci*. 1977;16:640–644.
6. Howell GR, Libby RT, Jakobs TC, et al. Axons of retinal ganglion cells are insulted in the optic nerve early in DBA/2J glaucoma. *J Cell Biol*. 2007;179:1523–1537.
7. Moore D, Harris A, Wudunn D, Kheradiya N, Siesky B. Dysfunctional regulation of ocular blood flow: a risk factor for glaucoma? *Clin Ophthalmol*. 2008;2:849–861.
8. Quigley HA. Optic nerve damage in human glaucoma. *Arch Ophthalmol*. 1981;99:635, doi:10.1001/archopht.1981.03930010635009.
9. Sigal IA, Ethier CR. Biomechanics of the optic nerve head. *Exp Eye Res*. 2009;88:799–807.
10. Sigal IA, Grimm JL, Jan N-J, Reid K, Minckler DS, Brown DJ. Eye-specific IOP-induced displacements and deformations of human lamina cribrosa. *Invest Ophthalmol Vis Sci*. 2014;55:1–15.
11. Campbell IC, Coudrillier B, Ross Ethier C. Biomechanics of the posterior eye: a critical role in health and disease. *J Biomech Eng*. 2014;136:021005.
12. Girard MJA, Dupps WJ, Baskaran M, et al. Translating ocular biomechanics into clinical practice: current state and future prospects. *Curr Eye Res*. 2015;40:1–18.
13. Midgett DE, Pease ME, Jefferys JL, et al. The pressure-induced deformation response of the human lamina cribrosa: Analysis of regional variations. *Acta Biomater*. 2017;53:123–139.
14. Quigley HA. Reappraisal of the mechanisms of glaucomatous optic nerve damage. *Eye*. 1987;1:318–322.
15. Burgoyne CF. A biomechanical paradigm for axonal insult within the optic nerve head in aging and glaucoma. *Exp Eye Res*. 2011;93:120–132.
16. Balaratnasingam C, Kang MH, Yu P, et al. Comparative quantitative study of astrocytes and capillary distribution in optic nerve laminar regions. *Exp Eye Res*. 2014;121:11–22.
17. Ishida T, Jonas JB, Ishii M, Shinohara K, Ikegaya Y, Ohno-Matsui K. Peripapillary arterial ring of Zinn-Haller in highly myopic eyes as detected by optical coherence tomography angiography. *Retina*. 2017;37:299–304.
18. Waisbourd M, Katz LJ. Selective laser trabeculoplasty as a first-line therapy: a review. *Can J Ophthalmol*. 2014;49:519–522.
19. Dikopf MS, Vajaranant TS, Edward DP. Topical treatment of glaucoma: established and emerging pharmacology. *Expert Opin Pharmacother*. 2017;18:885–898.
20. Schehlein EM, Novack GD, Robin AL. New classes of glaucoma medications. *Curr Opin Ophthalmol*. 2017;28:161–168.
21. Stowell C, Burgoyne CF, Tamm ER, Ethier CR, Lasker/IRRF initiative on astrocytes and glaucomatous neurodegeneration participants. Biomechanical aspects of axonal damage in glaucoma: a brief review. *Exp Eye Res*. 2017;157:13–19.
22. Tamm ER, Ethier CR, Lasker/IRRF Initiative on astrocytes and glaucomatous neurodegeneration participants. Biological aspects of axonal damage in glaucoma: a brief review. *Exp Eye Res*. 2017;157:5–12.
23. Hernandez MR. The optic nerve head in glaucoma: role of astrocytes in tissue remodeling. *Prog Retin Eye Res*. 2000;19:297–321.
24. Rogers RS, Dharsee M, Ackloo S, Sivak JM, Flanagan JG. Proteomics analyses of human optic nerve head astrocytes following biomechanical strain. *Mol Cell Proteomics*. 2012;11:M111.012302.
25. Exler RE, Guo X, Chan D, et al. Biomechanical insult switches PEA-15 activity to uncouple its anti-apoptotic function and promote ERK mediated tissue remodeling. *Exp Cell Res*. 2016;340:283–294.
26. Tehrani S, Davis L, Cepurna WO, et al. Astrocyte structural and molecular response to elevated intraocular pressure

occurs rapidly and precedes axonal tubulin rearrangement within the optic nerve head in a rat model. *PLoS One*. 2016;11:e0167364.
27. Wang R, Seifert P, Jakobs TC. Astrocytes in the optic nerve head of glaucomatous mice display a characteristic reactive phenotype. *Invest Ophthalmol Vis Sci*. 2017;58:924–932.
28. Levitzky M, Henkind P. Angioarchitecture of the optic nerve. II. Lamina cribrosa. *Am J Ophthalmol*. 1969;68:986–996.
29. Hayreh SS. The optic nerve head circulation in health and disease. *Ophthalmic Lit*. 1996;2:111.
30. Chang BL, Yamakawa T, Nuccio J, Pace R, Bing RJ. Microcirculation of left atrial muscle, cerebral cortex and mesentery of the cat. A comparative analysis. *Circ Res*. 1982;50:240–249.
31. Hudetz AG, Greene AS, Fehér G, Knuese DE, Cowley AW, Jr. Imaging system for three-dimensional mapping of cerebrocortical capillary networks in vivo. *Microvasc Res*. 1993;46:293–309.
32. Pittman RN. Influence of microvascular architecture on oxygen exchange in skeletal muscle. *Microcirculation*. 1995;2:1–18.
33. Goldman D, Popel AS. A computational study of the effect of capillary network anastomoses and tortuosity on oxygen transport. *J Theor Biol*. 2000;206:181–194.
34. Pittman RN. Oxygen transport in the microcirculation and its regulation. *Microcirculation*. 2013;20:117–137.
35. Gould IG, Tsai P, Kleinfeld D, Linninger A. The capillary bed offers the largest hemodynamic resistance to the cortical blood supply. *J Cereb Blood Flow Metab*. 2017;37:52–68.
36. Moody DM, Santamore WP, Bell MA. Does tortuosity in cerebral arterioles impair down-autoregulation in hypertensives and elderly normotensives? A hypothesis and computer model. *Clin Neurosurg*. 1991;37:372–387.
37. Brown WR, Thore CR. Review: Cerebral microvascular pathology in ageing and neurodegeneration. *Neuropathol Appl Neurobiol*. 2011;37:56–74, doi:10.1111/j.1365-2990.2010.01139.x.
38. Hughes S, Gardiner T, Hu P, Baxter L, Rosinova E, Chan-Ling T. Altered pericyte–endothelial relations in the rat retina during aging: implications for vessel stability. *Neurobiol Aging*. 2006;27:1838–1847.
39. Baloyannis SJ, Baloyannis IS. The vascular factor in Alzheimer's disease: a study in Golgi technique and electron microscopy. *J Neurol Sci*. 2012;322:117–121.
40. Patton N, Aslam T, MacGillivray T, Pattie A, Deary IJ, Dhillon B. Retinal vascular image analysis as a potential screening tool for cerebrovascular disease: a rationale based on homology between cerebral and retinal microvasculatures. *J Anat*. 2005;206:319–348.
41. Owen CG, Newsom RSB, Rudnicka AR, Barman SA, Woodward EG, Ellis TJ. Diabetes and the tortuosity of vessels of the bulbar conjunctiva. *Ophthalmology*. 2008;115:e27–e32.
42. Chan KKW, Tang F, Tham CCY, Young AL, Cheung CY. Retinal vasculature in glaucoma: a review. *BMJ Open Ophthalmol*. 2017;1:e000032.
43. Gaier ED, Wang M, Gilbert AL, Rizzo JF, Cestari DM, Miller JB. Quantitative analysis of optical coherence tomographic angiography (OCT-A) in patients with non-arteritic anterior ischemic optic neuropathy (NAION) corresponds to visual function. *PLoS One*. 2018;13:e0199793, doi:10.1371/journal.pone.0199793.
44. Jiang X, Johnson E, Cepurna W, et al. The effect of age on the response of retinal capillary filling to changes in intraocular pressure measured by optical coherence tomography angiography. *Microvasc Res*. 2018;115:12–19.
45. Numa S, Akagi T, Uji A, et al. Visualization of the lamina cribrosa microvasculature in normal and glaucomatous eyes: a swept-source optical coherence tomography angiography study. *J Glaucoma*. 2018;27:1032–1035.
46. Yang B, Brazile B, Jan N-J, Hua Y, Wei J, Sigal IA. Structured polarized light microscopy for collagen fiber structure and orientation quantification in thick ocular tissues. *J Biomed Opt*. 2018;23:1–10.
47. Yang B, Tunnell JW. Real-time absorption reduced surface fluorescence imaging. *J Biomed Opt*. 2014;19:90505.
48. Schindelin J, Arganda-Carreras I, Frise E, et al. Fiji: an open-source platform for biological-image analysis. *Nat Methods*. 2012;9:676–682.
49. Prada D, Harris A, Guidoboni G, Siesky B, Huang AM, Arciero J. Autoregulation and neurovascular coupling in the optic nerve head. *Surv Ophthalmol*. 2016;61:164–186.
50. Mozaffarieh M, Flammer J, eds. Pathogenesis of glaucomatous optic neuropathy. In: *Ocular Blood Flow and Glaucomatous Optic Neuropathy*. Springer Berlin Heidelberg; 2009;1:75–78.
51. Flammer J, Orgül S. Optic nerve blood-flow abnormalities in glaucoma. *Prog Retin Eye Res*. 1998;17:267–289.
52. Lee SH, Yu D-A, Kim T-W, Lee EJ, Girard MJA, Mari JM. Reduction of the lamina cribrosa curvature after trabeculectomy in glaucoma. *Invest Ophthalmol Vis Sci*. 2016;57:5006–5014.
53. Han H-C. Twisted blood vessels: symptoms, etiology and biomechanical mechanisms. *J Vasc Res*. 2012;49:185–197.
54. Ozturker ZK, Munro K, Gupta N. Optic disc hemorrhages in glaucoma and common clinical features. *Can J Ophthalmol*. 2017;52:583–591.
55. Kim Y-D, Han SB, Park KH, et al. Risk factors associated with optic disc haemorrhage in patients with normal tension glaucoma. *Eye*. 2010;24:567–572.
56. Arnold AC, Hepler RS. Fluorescein angiography in acute nonarteritic anterior ischemic optic neuropathy. *Am J Ophthalmol*. 1994;117:222–230, doi:10.1016/s0002-9394(14)73080-6.
57. Arnold AC, Badr MA, Hepler RS. Fluorescein angiography in nonischemic optic disc edema. *Arch Ophthalmol*. 1996;114:293–298.
58. Rizzo JF, 3rd. Unraveling the enigma of nonarteritic anterior ischemic optic neuropathy. *J Neuroophthalmol*. 2019;39:529–544.
59. Ohno-Matsui K, Kasahara K, Moriyama M. Detection of Zinn-Haller arterial ring in highly myopic eyes by simultaneous indocyanine green angiography and optical coherence tomography. *Am J Ophthalmol*. 2013;155:920–926.
60. Girard MJA, Strouthidis NG, Ethier CR, Mari JM. Shadow removal and contrast enhancement in optical coherence tomography images of the human optic nerve head. *Invest Ophthalmol Vis Sci*. 2011;52:7738–7748.
61. He X, Liu J. A quantitative ultrasonic spectroscopy method for noninvasive determination of corneal biomechanical properties. *Invest Ophthalmol Vis Sci*. 2009;50:5148–5154.
62. Ho LC, Sigal IA, Jan N-J, et al. Non-invasive MRI assessments of tissue microstructures and macromolecules in the eye upon biomechanical or biochemical modulation. *Sci Rep*. 2016;6:32080.
63. Palko JR, Morris HJ, Pan X, et al. Influence of age on ocular biomechanical properties in a canine glaucoma model with ADAMTS10 mutation. *PLoS One*. 2016;11:e0156466.
64. Voorhees AP, Ho LC, Jan N-J, et al. Whole-globe biomechanics using high-field MRI. *Exp Eye Res*. 2017;160:85–95.
65. Li Y, Xia X, Paulus YM. Advances in retinal optical imaging. *Photonics*. 2018;59.
66. Zhao Y, Li FM. Microangioarchitecture of optic papilla. *Jpn J Ophthalmol*. 1987;31:147–159.
67. Olver JM. Functional anatomy of the choroidal circulation: methyl methacrylate casting of human choroid. *Eye*. 1990;4:262–272.
68. Cioffi GA. Vasculature of the anterior optic nerve and peripapillary choroid. *The Glaucomas*. 1996;2:177–188.

69. Lieberman MF, Maumenee AE, Green WR. Histologic studies of the vasculature of the anterior optic nerve. *Am J Ophthalmol*. 1976;82:405–423.
70. Kang MH, Suo M, Balaratnasingam C, Yu PK, Morgan WH, Yu D-Y. Microvascular density is associated with retinal ganglion cell axonal volume in the laminar compartments of the human optic nerve head. *Invest Ophthalmol Vis Sci*. 2018;59:1562–1570.
71. Chuangsuwanich T, Moothanchery M, Yan ATC, Schmetterer L, Girard MJA, Pramanik M. Photoacoustic imaging of lamina cribrosa microcapillaries in porcine eyes. *Appl Opt*. 2018;57:4865.
72. Paula KY, McAllister IL, Morgan WH, Cringle SJ, Yu D-Y. Inter-relationship of arterial supply to human retina, choroid, and optic nerve head using micro perfusion and labeling. *Invest Ophthalmol Vis Sci*. 2017;58:3565–3574.
73. Hall JE. *Guyton and Hall Textbook of Medical Physiology - Pageburst E-Book on Vitalsource Retail Access Card*. Elsevier Health Sciences; 2015:167–303.
74. Herring N, Paterson DJ. *Levick's Introduction to Cardiovascular Physiology*. CRC Press; 2018:121–145.
75. Lucy KA, Wang B, Schuman JS, et al. Thick prelaminar tissue decreases lamina cribrosa visibility. *Invest Ophthalmol Vis Sci*. 2017;58:1751–1757.
76. Fuchsjäger-Mayrl G, Wally B, Georgopoulos M, et al. Ocular blood flow and systemic blood pressure in patients with primary open-angle glaucoma and ocular hypertension. *Invest Ophthalmol Vis Sci*. 2004;45:834–839.
77. Nakazawa T. Ocular blood flow and influencing factors for glaucoma. *Asia Pac J Ophthalmol (Phila)*. 2016;5:38–44.